

Simulation of Spray Combustion of *n*-Heptane in a Model Supersonic Combustor with Pilot Hydrogen

Zhiwei Huang, Majie Zhao, Huangwei Zhang

Department of Mechanical Engineering, National University of Singapore, 9 Engineering Drive 1, Singapore 117576, Republic of Singapore

1 Introduction

Liquid hydrocarbon fuels are more preferred in practical hypersonic propulsion systems, e.g. in supersonic combustion ramjets (scramjets) or scramjet-based combined-cycle engines, due to the advantages of easy storage and the potential of being a coolant [1,2]. However, combustion of liquid hydrocarbon fuels generally involves complex physical-chemical processes, such as injection, atomization, droplet breakup, evaporation, mixing, ignition, and flame stabilization. Presently, there are limited studies about the spray combustion characteristics under supersonic conditions.

The ignition delay time of hydrocarbon fuels is much longer than that of hydrogen, while the flame speed of the former is smaller. Therefore, flame stabilization of liquid hydrocarbon fuels in supersonic flows is challenging. Flame stabilization of hydrocarbon fuels can be enhanced by increasing the characteristic scale of the flame stabilization device [3], by using swirl atomizers [4], and by providing a pilot flame [2,5], etc. In this study, hydrogen is used as a pilot flame to stabilize a spray *n*-heptane (C_7H_{16}) jet in a model supersonic combustor. The combustor only with hydrogen injection was experimentally investigated by Waidmann et al. at the German Aerospace Center (DLR) [6]. For brevity, we termed this burner as DLR combustor hereafter in this paper. The focus of our work is to numerically investigate the combustion and stabilization characteristics of spray *n*-heptane flames in this supersonic DLR combustor.

A great difference between this burner and the one we studied previously [2] is that there was a hot burned rocket before ignition of the liquid hydrocarbon fuel in the latter. In such case, flame stabilization is not threatened with significant difficulty. However, in this study liquid *n*-heptane is injected simultaneously with hydrogen both at room temperature. Flame stabilization strongly depends on the air inflow conditions, combustor geometry, and injection parameters of the dual fuels, which needs further investigations. The authors are motivated to study the combustion and flame stabilization characteristics of hydrocarbon fuels at “cold” injection conditions.

2 Governing Equations

Governing equations for compressible turbulent combustion in gas phase are the conservation laws of mass, momentum, energy, and species. The liquid phase is modeled as a large number of tracked spherical droplets, with exchanges of mass, momentum, energy, and species with the continuous phase. The interaction among droplets is neglected since a dilute spray is assumed here, in which the volume fraction of the dispersed phase is typically less than 0.001 [7].

The governing equation of the droplet mass reads

$$\frac{dm_p}{dt} = \dot{m}_p. \quad (1)$$

The evaporation rate, \dot{m}_p , is estimated through

$$\dot{m}_p = -\dot{m}_f A_p, \quad (2)$$

where A_p is the droplet surface area and \dot{m}_f is the mass flux of vapor evaporating from the droplet into the gas phase, which is calculated as

$$\dot{m}_f = k_c M_p (c_s - c_\infty), \quad (3)$$

where k_c is the mass transfer coefficient, M_p is the molecular weight of the vapor, and c_s is the vapor concentration at the droplet surface. c_s is evaluated under the assumption that the partial pressure of the vapor at the droplet surface is same to the saturated pressure at the droplet temperature, and is calculated from

$$c_s = p_{sat} / RT_p, \quad (4)$$

where T_p is the droplet temperature, p_{sat} is the saturated pressure at T_p , and R is the universal gas constant. The concentration of vapor in the surrounding gas c_∞ in Eq. (3) is obtained from

$$c_\infty = X_i \cdot p / RT_\infty, \quad (5)$$

where X_i is the local mole fraction of the vapor, p and T_∞ are the local pressure and temperature of the gas, respectively. The mass transfer coefficient k_c in Eq. (3) is calculated from the Sherwood number [8]

$$Sh_{ab} = k_c d_p / D_{ab} = 2.0 + 0.6 Re_p^{1/2} Sc^{1/3}, \quad (6)$$

where d_p is the droplet diameter, D_{ab} is the vapor diffusivity in the gas, Re_p is Reynolds number of the droplet. Sc is the Schmidt number and $Sc = \nu / D_{ab}$, where ν is the kinematic viscosity of the gas.

The momentum equation of the droplet phase is written as

$$\frac{du_{i,p}}{dt} = \frac{F_{i,d}}{m_p}. \quad (7)$$

Here, we only consider the Stokes drag acting on the droplets, which is modeled based on the assumption of spherical droplets [9].

The energy equation of the droplet phase is

$$c_p \frac{dT_p}{dt} = \frac{Q_c + Q_{lat}}{m_p}. \quad (8)$$

where Q_c is the convective heat transfer between the droplet and the gas, $Q_c = hA_p(T_\infty - T_p)$. Here, h is the convective heat transfer coefficient. It is computed using the correlation of Ranz and Marshall [8]. Q_{lat} in Eq. (7) is the latent heat of n -heptane vaporization.

Two-way coupling between the liquid droplet phase and gas phase is taken into consideration, in terms of mass, momentum, energy and species. The governing equations of gas and droplet phases are solved using sprayRhoCentralFoam, which is developed based on rhoCentralFoam in OpenFOAM 5.0 package [10].

3 Computational Details

Two-dimensional configuration is chosen here to reduce the computational cost, which can still capture the main flow and combustion characteristics observed from experiments [11–13]. The combustor is 0.05 m in height at the entrance with a total length of 0.34 m. The strut is 0.032 m in length and 0.006 m in height for fuel injection and flame stabilization. Detailed dimensions of the combustor and the strut can be found in Refs. [6,14]. Three meshes with 55800, 220925, and 491700 structured cells are used for grid-dependence analysis and are denoted as M1, M2, and M3, respectively. Liquid n -heptane is then injected through the hydrogen injector at the strut base. Air and hydrogen inflow conditions and droplet injection parameters are listed in Table 1, in which $\phi_{p,i}$ is the partial global equivalence ratio for fuel i . The low ϕ_{p,H_2} is just taken from the experiment, and $\phi_{p,C_7H_{16}}$ is low because that the more C_7H_{16} injected, the more difficult the flame is to be stabilized.

Table 1: Inflow conditions for the hydrogen piloted spray combustion case

Inlet	p (Pa)	T (K)	Ma	u_x (m/s)	$\phi_{p,i}$
Air	100000	340	2.0	730	-
Hydrogen	100000	250	1.0	1200	0.034
n -heptane	-	298.15	-	1200	0.048

The initial droplet diameter is assumed to be 20 μm , while the initial droplet temperature is 298.15 K. Radiation, atomization, and breakup of the droplets are neglected. A global mechanism containing 6 species (e.g. O_2 , H_2 , C_7H_{16} , CO_2 , H_2O , and N_2) and 2 reactions is used for H_2/C_7H_{16} oxidation. The reaction steps and the rate constants are presented in Table 2.

Table 2: Two-step global mechanism for H_2/C_7H_{16} (units in cm^3 , mol, s, cal, and K)

Number	Reaction	A	n	Ea
1	$H_2 + 0.5O_2 \Rightarrow H_2O$	4.74×10^{12}	0.0	10063.8
2	$C_7H_{16} + 11O_2 \Rightarrow 7CO_2 + 8H_2O$	5.00×10^{08}	0.0	15780.0

4 Results and Discussions

4.1 Validation

Figure 1 shows the distributions of time-averaged axial velocity and temperature for the three meshes at different cross-sections in the combustor. Note that here only hydrogen combustion is considered due to no detailed experimental data are found for supersonic spray combustion in open literature to the authors' knowledge. Generally, meshes M2 and M3 give better predictions than M1. The large deviation of velocity and temperature in the recirculation zone is due to the simplification of the three-dimensional combustor to a two-dimensional one, in which a very narrow slot for hydrogen injection is adopted to

make the global equivalence ratio consistent with the experimental counterpart. It is seen that results from mesh M2 is close to those of M3 at most locations, and therefore they are used for the following analysis.

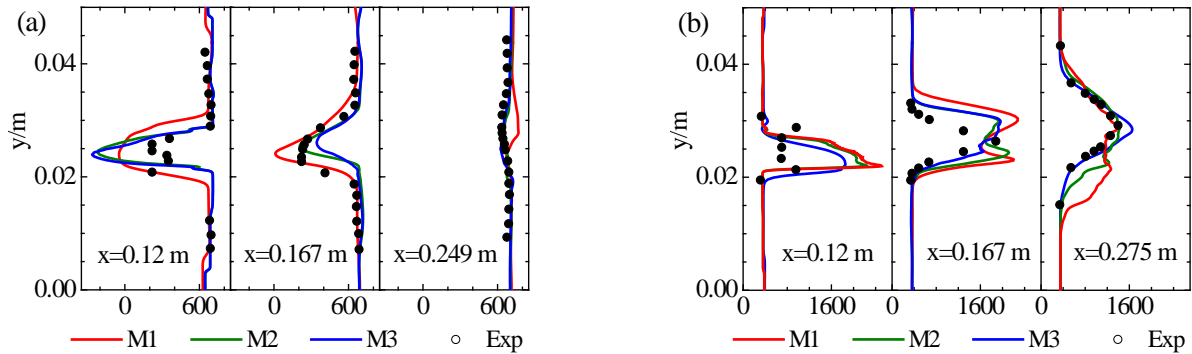


Figure 1. Comparisons of time-averaged (a) axial velocity (in m/s) and (b) temperature (in K) for the three meshes with experimental data [6]

4.2 Droplet Evaporation and Its Interactions with Gas Phase

Figure 2 shows the contours of droplet volume fraction (in logarithm scale) and C_7H_{16} vapor mass fraction in the entire combustor. The droplets are localized and mainly follow the vortical structures behind the strut. It is seen that $Y_{C_7H_{16}}$ can be as high as 50% after the strut in the recirculation zone. This is due to the long residence time of droplets dispersed in the recirculation zone, which will be shown clearly in Fig. 4. After about $x = 0.158$ m, $Y_{C_7H_{16}}$ decreases rapidly due to the reaction of C_7H_{16} (see Fig. 6b).

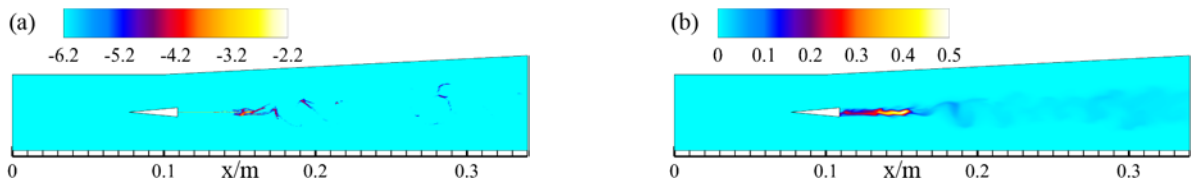


Figure 2. (a) Volume fraction of n -heptane droplets (in logarithm scale) and (b) mass fraction of C_7H_{16} vapor

Figure 3 shows the mass transfer rate due to droplet evaporation and convective heat transfer rate. Note that mass is transferred from the droplet to the gas, and heat is transferred in the reversed direction. The region with high droplet evaporation rate is in good accordance with that with high mass fraction of C_7H_{16} vapor. The droplet diameter decreases downstream (see Fig. 4), and the evaporate rate decreases as well. However, as intense combustion occurs downstream which leads to high gas temperature, the convective heat transfer between two phases gets stronger.

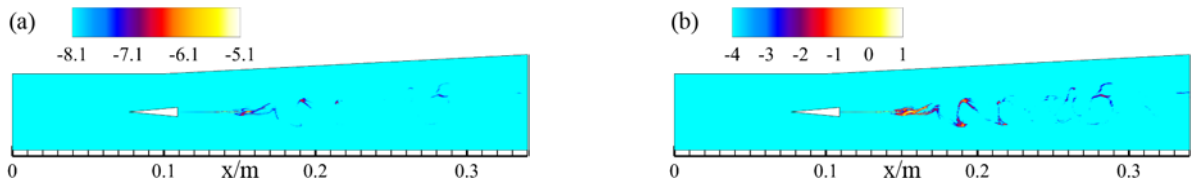


Figure 3. Rates of (a) mass transfer (kg/s) and (b) heat transfer (J/s) between two phases, in logarithm scale

Figure 4 shows the time history and diameter of the droplets in the combustor. It is seen that some droplets (within the red ellipse in Fig. 4a) at the end of the recirculation zone is trapped by the reversed flow,

whose residence time is much longer than the recently injected droplets at the adjacent upstream. The diameter of these trapped droplets is much smaller than the initial value ($20\ \mu\text{m}$). The evaporation from these long-time trapped droplets contributes to the high mass fraction of C_7H_{16} vapor in the recirculation zone.

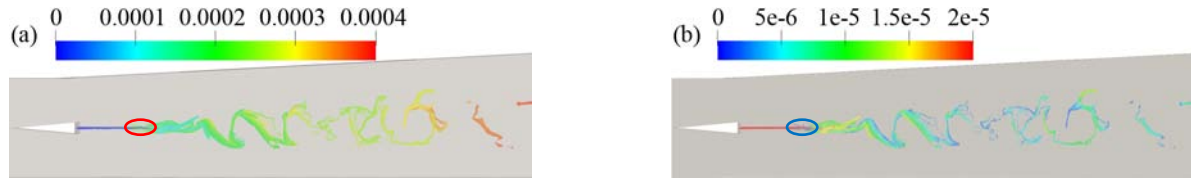


Figure 4. (a) The lifetime (in s) and (b) the diameter (in m) of the fuel droplets

4.3 Gaseous Combustion

Figure 5 shows the contours of gas temperature and axial velocity in the combustor. The high temperature flame starts at about $x = 0.14\ \text{m}$ with a reaction induction distance of $0.03\ \text{m}$ after the strut. Then the gas temperature increases rapidly and promotes the heat transfer between the two phases significantly. The recirculation zone with $u_x < 0$ filled with pink flood in Fig. 5(b), is seen to have a length of more than $0.05\ \text{m}$ after the strut. Some droplets are trapped in the recirculation zone and results in a long evaporation time. However, the reaction of C_7H_{16} is still weak (see Fig. 6) due to the low gas temperature there. Therefore, $Y_{\text{C}_7\text{H}_{16}}$ is high in the recirculation zone as shown in Fig. 2(b). Through comparing Figs. 5(a) and 5(b), it can be seen that a high temperature flame front is stabilized in the strut recirculation zone at about $x = 0.14\ \text{m}$, which then acts as the flame base for the downstream combustion.

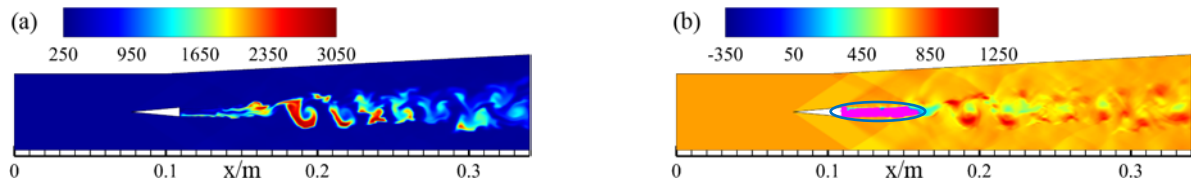


Figure 5. (a) Temperature (in K) and (b) axial velocity (in m/s) of the gas phase

Figure 6 shows the reaction rates (i.e. consumption rates) of H_2 and C_7H_{16} vapor. It is clearly seen that H_2 mainly reacts at the early stage in the combustor after the strut, while C_7H_{16} is mainly consumed further downstream (beyond the recirculation zone). The induction distance of C_7H_{16} is long even the upstream H_2 flame has provided it a high temperature atmosphere. There must be a balance between the combustion of H_2 and C_7H_{16} , beyond which the C_7H_{16} vapor cannot be effectively ignited. This is why we choose a low global equivalence ratio to initiate our research.

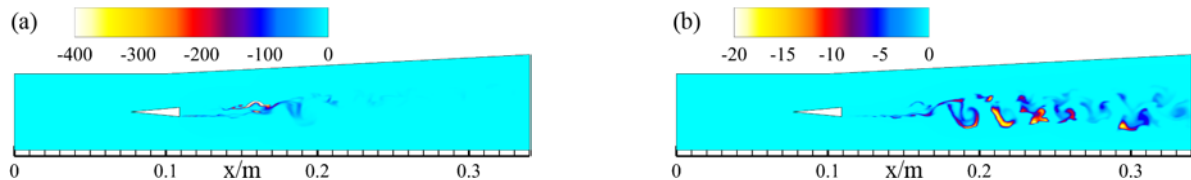


Figure 6. The reaction rates (in $\text{kg}/\text{m}^3/\text{s}$) of (a) H_2 and (b) C_7H_{16} vapor

5 Conclusions

Simulation of the spray combustion process of *n*-heptane is performed in a strut-based model supersonic combustor piloted with hydrogen. The solver is validated with experimental data on three different meshes for purely gaseous hydrogen combustion. Computational strategy is developed for modeling of spray combustion of liquid hydrocarbon fuels in supersonic flows. The pilot hydrogen flame in the recirculation zone is important for the liquid fuel evaporation, pre-heating, and the reaction induction of the liquid hydrocarbon fuel. Droplets trapped in the recirculation zone provide pre-evaporated and pre-heated high temperature vapor for further downstream combustion.

References

- [1] Ren ZX, Wang B, Xiang GM, Zhao D, Zheng LX. (2019). Supersonic spray combustion subject to scramjets: Progress and challenges. *Prog. Aerosp. Sci.* <https://doi.org/10.1016/j.paerosci.2018.12.002>.
- [2] Huang ZW, He GQ, Qin F, Cao DG, Wei XG, Shi L. (2016). Large eddy simulation of combustion characteristics in a kerosene fueled rocket-based combined-cycle engine combustor. *Acta Astronaut.* 127: 326.
- [3] Zhang M, Hu Z, He G, Liu P. (2010). Large-eddy simulation of kerosene spray combustion in a model scramjet chamber. *Proc. IMechE. Part G: J. Aerosp. Eng.* 224: 949.
- [4] Yuan R, Kariuki J, Mastorakos E. (2018). Measurements in swirling spray flames at blow-off. *Int. J. Spray Combust.* 10: 185.
- [5] Demosthenous E, Borghesi G, Mastorakos E, Cant RS. (2016). Direct numerical simulation of premixed methane flame initiation by pilot *n*-heptane spray autoignition. *Combust. Flame.* 163: 122.
- [6] Waidmann W, Alff F, Brummund U, Böhm M, Clauss W, Oschwald M. (1996). Supersonic combustion of hydrogen/air in a scramjet combustion chamber. *Space Tech.* 15: 421.
- [7] Crowe C, Schwarzkopf J, Sommerfeld M, Tsuji Y. (2012). *Multiphase flows with droplets and particles.* CRC Press (ISBN 978-1-4398-4050-4).
- [8] Ranz WE, Marshall WR. (1952). Evaporation from Drops, Part I and Part II. *Chem. Eng. Prog.* 48: 173.
- [9] Liu AB, Mather D, Reitz RD. (1993). Modeling the effects of drop drag and breakup on fuel sprays. SAE Technical Paper 930072.
- [10] Greenshields CJ, Weller HG, Gasparini L, Reese JM. (2010). Implementation of semi-discrete, non-staggered central schemes in a colocated, polyhedral, finite volume framework, for high-speed viscous flows. *Int. J. Numer. Meth. Fluids.* 63: 1.
- [11] Wang HS, Shan FL, Piao Y, Hou LY, Niu J. (2015). IDDES simulation of hydrogen-fueled supersonic combustion using flamelet modeling. *Int. J. Hydrogen Energy.* 40: 683.
- [12] Kummitha OR, Suneetha L, Pandey KM. (2017). Numerical analysis of scramjet combustor with innovative strut and fuel injection techniques. *Int. J. Hydrogen Energy.* 42: 10524.
- [13] Wu K, Zhang P, Yao W, Fan XJ. (2019). Computational realization of multiple flame stabilization modes in DLR strut-injection hydrogen supersonic combustor. *Proc. Combust. Inst.* <https://doi.org/10.1016/j.proci.2018.07.097>.
- [14] Huang ZW, He GQ, Qin F, Wei XG. (2015). Large eddy simulation of flame structure and combustion mode in a hydrogen fueled supersonic combustor. *Int. J. Hydrogen Energy.* 40: 9815.